Pseudopotential band calculations along a symmetry axis: Central potential

1994 J. Phys.: Condens. Matter 6 1497

(http://iopscience.iop.org/0953-8984/6/8/008)

J. Phys.: Condens. Matter 6 (1994) 1497–1511. Printed in the UK

Pseudopotential band calculations along a symmetry axis: central potential

D Agassi and J B Restorff
Naval Surface Warfare Center, Silver Spring, MD 20903-5000, USA

Received 26 May 1993, in final form 22 November 1993

Abstract. A method for band-structure calculations along a symmetry axis is introduced. It entails a cylindrical-coordinate multipole expansion of the wavefunction and an exact reduction of the 3D Schrödinger equation into a set of 1D wave equations for the multipoles. Group-theoretic considerations and energy arguments imply good convergence, regardless of the unit-cell extension along the symmetry direction. Calculations of a test case, the band structure of PbSe along the [111] direction without spin–orbit coupling, demonstrate the method's good convergence. The method is expected to be particularly useful for structures highly anisotropic along a symmetry axis, e.g., superlattices.

1. Introduction

The advent of superlattice fabrication, i.e., the growth of layered structures with alternate constituents, poses new challenges to band-structure calculations. A major difficulty is the colossal unit-cell size of such structures. A similar difficulty arises for crystals with a complicated anisotropic structure. Other such examples currently actively researched are semiconductor–semiconductor and semiconductor–insulator interfaces and ferromagnetic layered structures [1]. To address this difficulty, in particular in conjunction with epitaxial semiconductor superlattices, several methods have been developed. A popular phenomenological approach is the envelope-function method, supplemented by a prescription for the boundary conditions across an interface [2]. Other methods involve *ab initio* calculations of a small supercell and the 'complex-band-energy' method [3]. In this work we introduce a new method for addressing the above difficulty, which is specifically tailored for phenomenological band calculations of highly anisotropic structures along, or near, a symmetry axis. The method is motivated by the observation that many important structures, such as epitaxial superlattices, *always* grow along a symmetry axis such as the [100] or the [111] axis.

The method is predicated on the usage of a local empirical pseudopotential [4] in a cylindrical-coordinate representation. It reduces the problem of solving the 3D Schrödinger wave equation to the numerically simpler problem of solving a 'small' set of coupled 1D wave equations. A particular advantage of the present method is its good convergence which, according to arguments below, is expected to be independent of the unit-cell extension in the symmetry-axis direction. Stated heuristically, whereas in a conventional bulk calculation the number of basis functions grows as N^3 with the unit cell size, where N is the number of basis functions (e.g., plane waves) needed for each direction in space, in the present method the number of basis functions grows as mN, where m is a 'small' number, see below. The present approach leads naturally to a cylindrical $k \cdot p$ approximation in terms of which

0953-8984/94/081497+15$19.50

bands with momenta slightly deviating from that of the symmetry axis are perturbatively calculable around the 'exact' high-symmetry-axis bands. This section of the band structure is necessary for computing physical observables along the symmetry axis. In the rest of this section we briefly describe the central elements of the method. Details are given in the subsequent sections.

Our starting point is the observation that anisotropic structures, such as epitaxial superlattices, entail a preferred spatial direction, which is a symmetry axis. This suggests the introduction of cylindrical coordinates, where the z-axis coincides with the system's symmetry axis. In this representation, any lattice-periodic function $f(\boldsymbol{r})$, e.g. a pseudopotential, can be exactly expanded in terms of cylindrical multipoles $f_l(g, z')$ (section 2):

$$f(\boldsymbol{r}) = \sum_{l=-\infty}^{\infty} \sum_{g} f_l(g, z') J_l(g\rho) e^{il\phi} \tag{1.1}$$

where ρ, ϕ, z' are the standard cylindrical coordinates, $J_l(x)$ is the Bessel function of integer order l, and g is a non-negative label that runs over an infinite series specific to the geometry of the reciprocal vector space (it is the length of the transverse (normal to z') reciprocal lattice vectors). As (1.1) shows, the ϕ and ρ (transverse) dependence is carried by standard functions. Consequently, the analysis is focused on solving for the single-variable multipoles—the 'guts' of $f(\boldsymbol{r})$. Spin degrees of freedom are covered in a subsequent paper.

The good convergence of (1.1) is a consequence of severe constraints on the l and g labels due to group-theoretical and energy considerations. To demonstrate these, consider a rocksalt structure along the [111] direction. As shown in section 3, the proper group symmetry implies that only *two* l values need be considered! This renders (1.1), in effect, an expansion in ascending g values. The g label, in turn, determines the number of transverse (normal to z') nodes via the oscillatory Bessel function. Consequently, for a given band energy, all g values up to a cut-off value g_c are expected to contribute. A crude estimate of g_c is obtained as follows. The 'low'-energy bands (near the Fermi level, in the spirit of the pseudopotential method) have the *least* number of ρ-oscillations inside the unit cell. For $l > 0$, $J_l(g\rho)$ rises from $J_l(0) = 0$ to a maximum at $\rho \simeq (l + \frac{3}{2})/g$ and henceforth oscillates with a period $1/g$ [5]. (For $l = 0$, the latter oscillations start at $\rho = 0$.) Therefore, the *lowest* bands have no ρ-oscillations inside the unit cell. The condition for this is therefore $(l_m + \frac{3}{2})g_c \simeq a_T$, where a_T is a typical *transverse* unit cell extension and l_m is a typical l value. (Since only two l values enter, l_m is easily estimated.) For the test case of bulk PbSe (section 5) $l_m = 3$, $a_T \simeq a/2 = 3$ Å where a is the lattice constant. This gives $g_c \simeq 1.5$ Å^{-1}, which is approximately the second g value (table 1). Thus, only about four terms in (1.1) need be considered. These considerations demonstrate that the number of relevant multipoles is 'small', and can be estimated prior to calculations. As shown in section 5 this estimate is actually quite good. Note that it is a_T that is involved in the g_c estimate. Therefore the above consideration *applies equally* to a superlattice in the [111] direction, since the transverse projection of the lattice constant is the same for the bulk and the superlattice. Numerical demonstration of the latter statement is deferred to future work.

The cylindrical multipoles satisfy an exact set of *one-dimensional*, coupled wave equations (section 4):

Table 1. The allowed g-values and the hexagon-tile angle $\Phi_0(g)$ (3.1) for an FCC lattice and the [111] direction.

	f	g(PbSe)[a] (Å^{-1})	$\Phi_0(g)$ (°)
1.	0	0	0
2.	$10.2606 = 2\pi\sqrt{8/3}$	1.6754	0
3.	$17.7714 = 2\pi\sqrt{8}$	2.9018	30
4.	$20.5207 = 2\pi\sqrt{32/3}$	3.3507	0
5.	27.1465	4.4326	19.1066
6.	30.7813	5.0261	0
7.	35.5430	5.8036	30
8.	36.9944	6.0406	13.8979

[a] We used [16] a(PbSe, T = 300 K) = 6.1243 Å.

$$\left(-g_0^2+\frac{2m_0}{\hbar^2}E(k)+\frac{\mathrm{d}^2}{\mathrm{d}z'^2}\right)\Psi_l(g_0,z')+\sum_{g_P,g_F}\sum_{m=-2}^{3}A_{l,m}(g_0,g_P,g_F)\left(-\frac{2m_0}{\hbar^2}v_m(g_P,z')\right)\times\Psi_{l-m}(g_F,z')=0 \tag{1.2}$$

where $\Psi_l(g, z')$ and $v_m(g_P, z')$ are the wave function (unknown) and the local pseudopotential (known) multipoles, respectively. The A-coefficients $A_{l,m}(g_0, g_P, g_F)$ are geometrical coefficients determined by the lattice point group and the z'-axis symmetry. The A-coefficients, to our knowledge, are new constructs that embody the transverse crystal-momenta vector-addition geometry. They are analogous to the Clebsch–Gordan coefficients associated with angular momenta addition. The one-dimensionality of (1.2) is numerically advantageous when dealing with an extended unit cell in the symmetry-axis direction.

The good convergence of (1.1) is verified numerically for the test case of bulk PbSe, without spin–orbit coupling, along the entire Brillouin zone [111] line (section 5). This choice is motivated by its direct L-point band gap, which implies a preferred symmetry axis and a gap at a high-symmetry point. This example is consistent with the theme of this work, i.e., to introduce the new method and check its merit for a non-trivial case. Calculations of more complex systems and lower symmetry, such as indirect semiconductors and semiconductor superlattices, are deferred to future studies.

The paper is organized as follows. In section 2 we introduce the multipole expansions for the pseudopotential and the wave function. Section 3 is devoted to the discussion of symmetry constraints on the multipole expansion. In section 4 we derive the basic set of coupled wave equations. The numerical results for bulk PbSe bands in the Γ–Λ–L direction are given in section 5. Section 6 is a summary and brief discussion. The considerable mathematical detail has been published elsewhere [6].

2. Cylindrical multipole expansion

As in other versions of the empirical pseudopotential approach, the computational task is to solve the 3D Schrödinger equation with a given local periodic potential. Unlike other approaches, however, a cylindrical coordinate system is introduced here from the outset by

choosing the z-axis along a crystal high-symmetry axis. For the sake of specificity it is hereafter assumed that this axis is the [111] direction of a rocksalt or zincblende lattice.

The primed coordinates, where $\hat{z}' \parallel [111]$, are given by

$$(r) = \mathbf{R}(r) \tag{2.1}$$

where $\mathbf{R}$ in (2.1) is the rotation matrix. By the same token, denoting the reciprocal lattice vectors in the unprimed coordinates by $G = (G_x, G_y, G_z)$, the vector's components in the primed coordinates $G = (G'_x, G'_y, G'_z)$ are given by the transformation (2.1). The cylindrical coordinates pertinent to the primed coordinates (x', y', z') are conventionally defined by

$$x' = \rho \cos \phi \qquad y' = \rho \sin \phi \qquad z' = z'. \tag{2.2}$$

To introduce the multipole expansion of a lattice-periodic function consider the expansion of a local empirical pseudopotential $v(r)$ [4, 7]

$$v(r) = \sum_G v(G) e^{iG \cdot r} = \sum_{G'} v'(G') e^{iG' \cdot r'} = v'(r') \tag{2.3}$$

where $v'(G') \equiv v(G(G'))$. Expansion (2.3) is obviously valid for any lattice periodic function. The argument in the exponent of (2.3), transcribed to the cylindrical coordinates (2.2), is

$$G' \cdot r' = \rho g_P \cos\bigl(\phi - \delta(G'_T)\bigr) + G'_z z' \tag{2.4}$$

where the azimuthal shift angle $\delta(G'_T)$ and the transverse reciprocal lattice momentum length g_P are defined by

$$\cos \delta(G'_T) = G'_x / g_P \qquad \sin \delta(G'_T) = G'_y / g_P \qquad g_P = \sqrt{G'^2_x + G'^2_y} \tag{2.5}$$

and $G'_T = (G'_x, G'_y)$. For the $g_P = 0$ case we adopt the convention $\delta(G'_T) = 0$. The particular G vectors for an FCC lattice [8] yield the g_P values of table 1.

With these preliminaries, the multipole expansion of $v(r)$ is derived by employing the identity [9]

$$e^{iz \cos \phi} = \sum_{l=-\infty}^{\infty} i^l J_l(z) e^{il\phi} \tag{2.6}$$

to the RHS of the exponential in (2.3), employing (2.4). These steps yield

$$v'(r') = \sum_{g_P} \sum_{l=-\infty}^{\infty} v_l\bigl(g_P, z'\bigr) J_l\bigl(g_P \rho\bigr) e^{il\phi} \tag{2.7a}$$

where the multipoles are given by

$$v_l\bigl(g_P, z'\bigr) = i^l \sum_{G' : |G'_T| = g_P} v'(G') e^{iG'_z z'} e^{-il\delta(G'_T)} \tag{2.7b}$$

The summation in (2.7b) implies summation over all G' such that the length of G'_T has the prescribed value g_P. Note that since $J_l(0) = \delta_{l,0}$, it follows that $v_l(g_P = 0, z') = \delta_{l,0} v_0(0, z')$.

A similar analysis is now applied to a band wavefunction $\Psi_{nk}(r)$ [10]:

$$\Psi_{nk}(r) = e^{ik\cdot r} f_{nk}(r) \qquad f_{nk}(r) = \sum_{L} \Psi_{nk}(L) e^{iL\cdot r} \tag{2.8}$$

where $f_{nk}(r)$ is lattice periodic. When transformed to the primed coordinates, the function $f_{nk}(r)$ is expanded as in (2.7), while the exponential factor takes the form $\exp[ik\cdot r] = \exp[ik'\cdot r'] = \exp[ik'z']$ for k vectors pointing in the symmetry axis direction. For such k vectors—*the only k vectors considered hereafter*—the wavefunction multipole expansion is

$$\Psi_{nk}(r) = \sum_{g_F} \sum_{l=-\infty}^{\infty} \Psi_{nl}(g_F, k', z') J_l(g_F \rho) e^{il\phi}$$

$$\Psi_{nl}(g_F, k', z') = i^l \sum_{L':|L'_T|=g_F} \Psi_{nk'}(L') e^{i(L'_z + k')z'} e^{-il\delta(L'_T)}. \tag{2.9}$$

The shift angle $\delta(L'_T)$, reciprocal lattice momentum length g_F and summation convention in (2.9) are as in (2.5) and (2.7). The notation in (2.9) is simplified hereafter by omitting the k', n labels, i.e. $\Psi_{nl}(g_F, k', z') = \Psi_l(g_F, z')$.

The attractive feature of expansions (2.7) and (2.9) is that each multipole lumps together the contribution of many plane waves, all of which share the same length of the transverse reciprocal vector. Hence few such multipoles may be sufficient to describe low bands.

3. Symmetry properties

Having established the multipole expansion structure we turn now to discuss the associated label l. As is demonstrated below, the l values are determined by the particular structure and symmetry of the crystal.

Consider first the allowed g values, table 1, and the locus of G'_T. All G'_T of given length g span hexagons, which are either single or a pair, symmetrically tilted with respect to the G'_x axis [6]. The tilting angle, denoted by $\Phi_0(g)$, is given in table 1. Consequently, the shift angle $\delta(G'_T)$ (2.5) has the form

$$\delta(G'_T) = \pm[\Phi_0(g) + (\pi/3)j) \qquad j = -2, -1, 0, \ldots, 3. \tag{3.1}$$

A $\Phi_0(g) = 0$ entry implies a 'single' hexagon. Upon inserting (3.1) in (2.9) one obtains an important phase relation among the wavefunction multipoles.

$$\Psi_{l\pm 6}(g_F, z') = -e^{\mp 6i\Phi_0(g_F)} \Psi_l(g_F, z') \qquad \text{when } \sin[6\Phi_0(g_F)] = 0. \tag{3.2}$$

Equation (3.2) (and similar unpublished relations, not needed for the example in section 5) implies that the number of *independent* l multipoles is six or less. This l-periodicity is a consequence of symmetry and a manifestation of the Bloch theorem in the transverse direction. The Bloch theorem in the longitudinal direction is introduced in the next section.

The axis symmetry restricts the allowed l-values in the wavefunction and pseudopotential multipole expansions. For the Γ–L direction, the relevant groups of wave vector k are C_{3v} and D_{3d} for a Δ point and the L point, respectively (the latter for the rocksalt structure

only) [11]. As outlined now for the Δ point, these group symmetries restrict the allowed l-values [6]. Starting from a general multipole expansion

$$\Psi(r') = \sum_{l=-\infty}^{\infty} \Psi_l(\rho, z')e^{il\phi} \tag{3.3}$$

applying the $X_{\pm 1}$ and Y_0 group operators [6, 12] to (3.3) and equating the result to the corresponding irreducible representation, it follows that $l = 3m$, where $m = 0, \pm 1, \pm 2, \ldots$ and the l-parity is

$$\Psi_{-l}(\rho, z') = \epsilon \Psi_l(\rho, z') \tag{3.4}$$

where $\epsilon = +1$ and $\epsilon = -1$ for the Λ_1 and Λ_2 representations, respectively. In a similar manner we proceed for the other irreducible representations. Table 2 gives the l-sequences for all relevant representations [6]. At the L point the D_{3d} group of wave vector k contains the C_{3v} operations and z'-inversion. Consequently, the corresponding multipoles in table 3 have also a definite phase relation between $\Psi_l(\rho_F, z')$ and $\Psi(g_F, -z')$.

Table 2. The allowed l-values and l-parity for the group C_{3v}.

Irreducible representation	l-values[a]	l-parity π_l[b]
Λ_1	$\|1\rangle$: $l = 3m$	$(-1)^l$
Λ_2	$\|1\rangle$: $l = 3m$, $m \neq 0$	$-(-1)^l$
Λ_3	$\|1\rangle$: $l = 3m+1$	$-\begin{bmatrix} 0 & (-1)^m \\ (-1)^m & 0 \end{bmatrix}$
	$\|2\rangle$: $l = 3m-1$	

[a] $m = 0, \pm 1, \pm 2, \ldots$.

[b] $\Psi_{-l}(g, z') \equiv \pi_l(\Psi_l(g, z'))$ where $\Psi_l(g, z') = \Psi_l(g, z')$ or $\begin{bmatrix} \Psi_l^{(1)}(g, z') \\ \Psi_l^{(2)}(g, z') \end{bmatrix}$.

Table 3. The allowed l-values, l-parity and z-parity for the group D_{3d}.

Irreducible representation	l-values[a]	l-parity π_l[b]	z-parity π_z[c]
L_1	$\|1\rangle$: $l = 3m$	$(-1)^l$	$(-1)^l$
L_2	$\|1\rangle$: $l = 3m$, $m \neq 0$	$-(-1)^l$	$(-1)^l$
L_1	$\|1\rangle$: $l = 3m$, $m \neq 0$	$-(-1)^l$	$(-1)^l$
L_2'	$\|1\rangle$: $l = 3m$	$(-1)^l$	$-(-1)^l$
L_3	$\|1\rangle$: $l = 3m+1$	$-\begin{bmatrix} 0 & (-1)^m \\ (-1)^m & 0 \end{bmatrix}$	$-\begin{bmatrix} (-1)^m & 0 \\ 0 & (-1)^m \end{bmatrix}$
	$\|2\rangle$: $l = 3m-1$		
L_3'	$\|1\rangle$: $l = 3m+1$	$-\begin{bmatrix} 0 & (-1)^m \\ (-1)^m & 0 \end{bmatrix}$	$\begin{bmatrix} (-1)^m & 0 \\ 0 & (-1)^m \end{bmatrix}$
	$\|2\rangle$: $l = 3m-1$		

[a] $m = 0, \pm 1, \pm 2, \ldots$.

[b] $(\Psi_{-l}(g, z')) \equiv \pi_l(\Psi_l(g, z'))$ where $(\Psi_l(g, z')) = \Psi_l(g, z')$ or $\begin{bmatrix} \Psi_l^{(1)}(g, z') \\ \Psi_l^{(2)}(g, z') \end{bmatrix}$.

[c] $(\Psi_l(g, -z')) \equiv \pi_z(\Psi_l(g, z'))$.

The local pseudopotential (2.3) is by construction invariant under all space group operations; in particular it transforms as the scalar representation under the C_{3v} and D_{3d} operators, i.e., as the Δ_1 and L_1 representations [12], respectively.

The combination of the symmetry l-selection rules of tables 2 and 3 and the l-periodicity (3.2) restricts further the allowed l-sequences. Consider, for example, the pseudopotential. For the example of section 5, it turns out that only the four lowest g-values contribute substantially, hence (3.2) is valid and $0 \leqslant l < 6$. On the other hand, the pseudopotential transforms as the L_1 representation, hence, according to table 3, $l = 0, \pm 3, \pm 6, \ldots$. Consequently, only the *two* multipoles, $l = 0, 3$, need be considered since all the others are phase related! Similar symmetry considerations with regard to the wavefunction reduce drastically the number of independent multipoles (see section 5).

4. Coupled wave equations

In this section we outline the transcription of the Schrödinger equation into a set of equations for the multipoles. Details can be found in [6] and appendix A.

Transforming the Schrödinger equation to the primed coordinates, expressing the Laplacian in the cylindrical coordinates (2.3), inserting the wavefunction multipole expansion (2.9) and denoting the multipoles of the product $v'(r')\Psi_{nk}(r')$ by $X_l(g_0, z')$, simple projection manipulations give

$$\left[-g_0^2 + (2m_0/\hbar^2)E_n(k) + \mathrm{d}^2/\mathrm{d}z'^2\right]\Psi_l(g_0, z') - (2m_0/\hbar^2)X_l(g_0, z') = 0 \tag{4.1}$$

where m_0 is the electron mass and $E_n(k)$ is the band energy. To render (4.1) useful it is necessary to express $X_l(g_0, z')$ in terms of the known pseudopotential multipoles $v_l(g_P, z')$ and the unknown wavefunction multipoles $\Psi_l(g_F, z')$. This exercise constitutes the content of appendix A. It involves the geometry of adding the transverse (two-dimensional) momenta of the wavefunction and pseudopotential expansions, subject to the vector addition constraints depicted in figure 1. This is analogous to vector addition of angular momenta. The corresponding vector coupling coefficients, analogous to the Clebsch–Gordan coefficients, are denoted here by $A_{l,m}(g_0, g_P, g_F)$ and are given in table 4. The resulting multipole wavefunction is

$$\left[-g_0^2 + \frac{2m_0}{\hbar^2}E_n(k) + \frac{\mathrm{d}^2}{\mathrm{d}z'^2}\right]\Psi_l(g_0, z') + \sum_{g_P, g_F}\sum_{m=-2}^{3} A_{l,m}(g_0, g_P, g_F)\left[-\frac{2m_0}{\hbar^2}v_l(g_P, z')\right] \times \Psi_{l-m}(g_F, z') = 0 \tag{4.2}$$

where the multipoles $\Psi_l(g_F, z')$ satisfy the longitudinal Bloch theorem in the z' direction

$$\Psi_l(g_F, z' + a^*) = \mathrm{e}^{\mathrm{i}k'a^*}\Psi_l(g_F, z') \tag{4.3}$$

and k' and a^* are the [111]-projected lattice momentum and lattice constant, respectively, given by

$$k' = 3\pi K/a^* \qquad a^* = a\sqrt{3} \qquad 0 < K \leqslant 1. \tag{4.4}$$

The L and Λ points correspond to $K = 1$ and $K < 1$, respectively. Note the difference between the Bloch theorem in the z' direction (4.3) and that in the transverse direction (3.2).

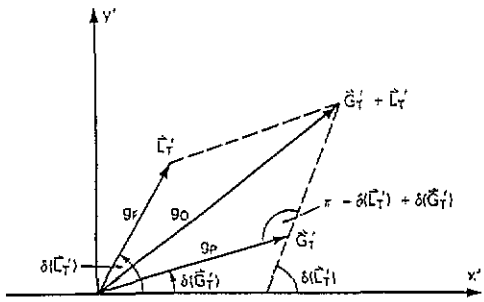

Figure 1. The transverse reciprocal vector parallelogram defining the notations used in section 4 and appendix A.

Table 4. The A-coefficients. The triangle configuration corresponds to figure 1. For a triad g_0, g_P, g_F to conform with the geometrical constraints of figure 1, the selection rules in note a must be satisfied. For all cases not quoted in the table $A_{l,m}(g_0, g_P, g_F) = 0$.

g_0	l	m	g_P, g_F	$A_{l,m}(g_0, g_P, g_F)$	$\lvert c\rvert$[a]	Triangle configuration
0	0	0	$g_P = g_F = 0$	1	∞	•
	0	a. al.[b]	$g_P = g_F \neq 0$	$\frac{1}{6}(-1)^m$	1	$\longleftarrow \longrightarrow$ $g_P \quad g_F$
$\neq 0$	a. al.[b]	0	$g_P = 0$, $g_F = g_0$	1	∞	$\longrightarrow\!\bullet$ $g_P \; g_F$
	a. al.[b]	l	$g_P = g_0$, $g_F = 0$	1	∞	$\bullet\!\longrightarrow$ $g_F \; g_P$
	a. al.[b]	a. al.[b]	$g_P \neq 0$, $g_G \neq 0$	$A_{l,m}^c$	$\leqslant 1$	$\overset{\nearrow}{\leftarrow\!\rightrightarrows}\rightarrow$ $g_P \quad g_F \quad \longrightarrow$

[a] $c = (g_0^2 - g_F^2 - g_P^2)/2g_Fg_P$, $|c| = 0, \frac{1}{2}, \frac{\sqrt{3}}{2}, 1, \infty$ for an FCC crystal and the [111] direction.
[b] a. al. = any allowed value.
[c] $A_{l,m}(g_0, g_F, g_F) = \frac{1}{3}W(|c|)\ \mathrm{Re}\,[B_l^{(+)}\exp(im|\cos^{-1}(c)|)]$, $B_l^{(+)} = (((g_F + g_P(c - i\sqrt{1-c^2}))/g_0)^l$, $W(|c|) = \frac{1}{2}$ for $|c| = 1$, $W(|c|) = 1$ for $|c| < 1$.

This underscores the different treatment of the longitudinal and transverse directions in the present cylindrical representation.

The coupled set of wave equations (4.2) is the central result of this work. These equations are exact for the [111] direction and rocksalt or zincblende structures (since both structures have the same reciprocal lattice [13]). The symmetry of the calculated band is determined by the chosen l-value sequence according to tables 2 and 3. The ascending g-value sequence is given in table 1. The selected g-values are determined by convergence considerations. An example for this paradigm is given in the next section.

Equations (4.2) are reminiscent of the Kronig–Penney model [14] except for the fact that it is a set of equations. The coupling between the 1D wave equations reflects the underlying 3D nature of the problem, unlike the strict one dimensionality in the Kronig–Penney model.

5. Band structure of 'PbSe' in the Γ–L direction

In this section the cylindrical multipole expansion method is numerically tested for bulk PbSe. All calculations were carried out on a modest PC (386/25, 4Mb memory). Typical

times for constructing the secular equation and evaluating its determinant are of the order of seconds. To eliminate round-off errors, which may blur convergence, double precision was used. We employed 15 plane waves per multipole, with up to six multipoles. This basis can be reduced in an optimized calculation [6].

Some of the motivation for choosing PbSe was mentioned in section 1. This narrow-gap semiconductor example offers a stringent test from the point of view of numerical convergence since the band gap is small (0.165 eV at $T = 4.2$ K), and is comparable to other band gaps in the band structure. It also offers the numerical advantage in that the band gap is located at a high-symmetry point (the L point). On the other hand, since PbSe is a heavy-element narrow-gap semiconductor, the spin–orbit interaction must be included to realistically represent the bands at the L point. Thus, our example of spinless PbSe, which employs a local pseudopotential (2.3)—hereafter denoted by 'PbSe'—cannot be directly compared to calculations with the spin–orbit interaction and a non-local central pseudopotential [7, 11, 16].

Comparing on the one hand the band structure of a non-local pseudopotential calculation [7] and a non-local *ab initio* calculation [11, reference 11], and on the other hand a local pseudopotential calculation [15, 16]—all with spin–orbit interaction—we note that all are very similar, in particular near the band gap. This outcome is interpreted to imply that, in the presence of spin–orbit interaction, non-locality in the central potential can be represented by an equivalent local pseudopotential. (The electron effective mass introduced in [7] is an example of such a procedure.) Provided the latter statement is also valid in the absence of the spin–orbit interaction, local pseudopotential calculations, as persued here, have the capacity of yielding the correct band structure near the band gap. With regard to the spin–orbit interaction, the few PbSe band-structure calculations in the absence of the spin–orbit interaction [7, figures 3, 11] all have in common the same band *sequence*, at the L point. Given all this, our criterion for a 'correctly' calculated band structure of 'PbSe' is that it reproduces the correct sequence and degeneracies of the low bands [7, figures 3, 11(a)] and is numerically convergent. Non-local effective-mass corrections [7] are not essential for the present purpose of a convergence study.

The input to the wave equations (4.2) are the pseudopotential's multipoles. The empirical pseudopotential for PbSe consists of the entries $v(G)$ (2.3) with $|G|^2 \leqslant 12(2\pi/a)^2$ [7]. The component with $|G|^2 = 16(2\pi/a)^2$ in [7] is omitted here partly since it is not included in a local pseudopotential calculation [15] and partly as a simplifying assumption. The corresponding g-values are the lowest four entries in table 1. From these $v(G)$-values we numerically construct all the non-vanishing pseudopotential multipoles using (2.7*b*). The results are given in figure 2. Note that the $v(G)$ coefficients (2.3) are products of a form factor $w(G)$ and a structure factor $S(G)$, where the former depends only on the magnitude of G, whereas the latter depends on the choice of an origin in the primitive unit cell.

The g-values for the wavefunction are at least those needed for the pseudopotential, i.e., the lowest four in table 1. To assess the importance of higher g-multipoles one uses a combination of symmetry and energy considerations and case-specific numerical calculations. Consider first the $g(5)$ multipole. As figure 2 shows, the $g(2)$ pseudopotential multipole is the dominating one. Hence, for the $g(5)$ wavefunction multipole to couple strongly to the *lower* four wavefunction multipoles, it must couple via the $g(2)$ pseudopotential multipole. Such a coupling term has to satisfy the geometrical constraints embodied in the A-coefficients (4.2). In addition, the 'unperturbed energy' of the $g(5)$ multipole should be not too different from that of the lower four multipoles already included in the calculation. This latter criterion is standard for determining important configuration mixing in atomic and nuclear eigenvalue calculations, and is based on minimizing energy

denominators in the perturbation-theory expression for the eigenvalue. From the wave equation (4.2) it is evident that the '$-g_0^2$' diagonal term plays the role of the 'unperturbed energy'. Now, a quick check of the A-coefficients shows that only the $g(4)$ couples to $g(5)$ via the $g(2)$ pseudopotential multiple. Therefore, for bands in which the $g(4)$ component is an important one, the $g(5)$ multipole should be considered and for bands in which the $g(4)$ multipole is unimportant, the $g(5)$ contribution can be safely ignored. The issue then is how important the $g(4)$ component is for the lowest bands. This question is numerically answered in figure 3(b), which shows the bands generated by including only the $g(1)$, $g(2)$ and $g(3)$ multipoles. Though the band sequence is not perfect everywhere, and the band gap is too large, the band sequence is essentially correct. This implies that these wavefunction multipoles are the most important ones. Hence the $g(4)$ multipole is *not* a prominent one for the lowest bands, and hence the $g(5)$ multiple can be ignored. In addition, with regard to the 'unperturbed energy' criterion, we find from table 1 that $(g(5)/g(4))^2 \simeq 1.7$, $(g(5)/g(2))^2 \simeq 7$ and $(g(4)/g(2))^2 \simeq 4$. These figures indicate that the $g(5)$-multipole 'unperturbed energy' is far removed from those of the lower four multipoles. This provides another argument for not including it in a lowest-four g-values calculation.

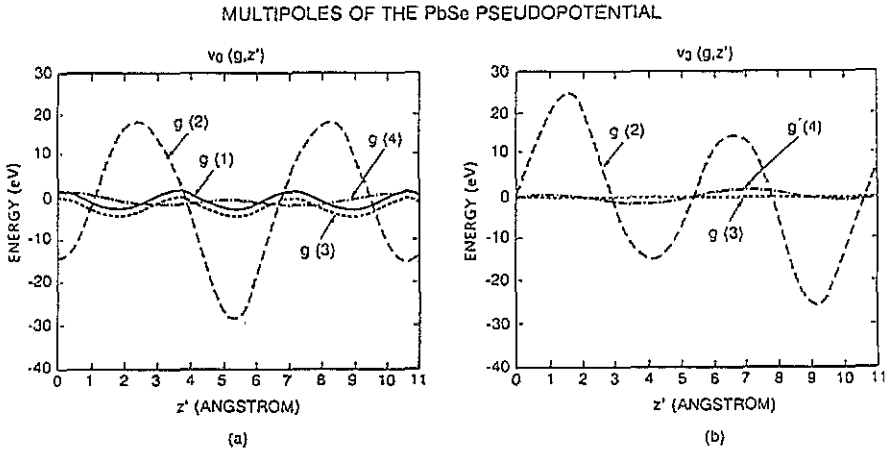

Figure 2. The pseudopotential multipoles for all l- and g-values, along the $\hat{z} \parallel [111]$ axis. The lattice constant in the [111] direction (4.4), is $a^* = 10.608$ Å.

Assessing the relevance of yet higher g-multipoles, e.g. $g(6)$, follows the same lines. Since $(g(6)/g(4))^2 \simeq 2.6$ and $(g(6)/g(2))^2 \simeq 9$, the unperturbed energy consideration implies that the contribution of $g(6)$ and higher g-values to the lowest bands is negligible. This type of argument illustrates how the ascending g-value series is naturally truncated with a modest amount of numerical work. It also indicates that the sparser the g-value series is, the faster the low-band multiple-expansion series converges.

The results for the L point are compiled in table 5, and for the entire Γ–L line are depicted in figure 3. The equations for the L_1, L_2', and the L_3, L_3' bands decouple and hence are solved separately. As discussed above, a sufficient base for the calculations is the $g(1)$, $g(2)$, $g(3)$, $g(4)$ wavefunction multipoles and two l-values. The quality of the calculated band structure is established by comparing with the band sequence in [7] and [11] and numerical convergence.

Consider first table 5 and figure 3(a). Note that already at the level of including only $g(1)$, $g(2)$ the correct features of the L_1, L_2' band structure are reproduced throughout the

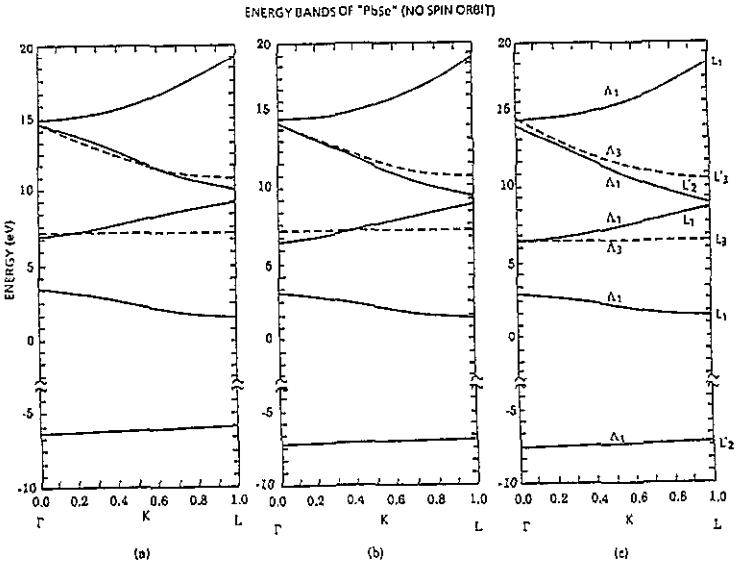

Figure 3. *The calculated band structure of 'PbSe' in the Γ–L direction (no spin–orbit* interaction). The solid lines are the L_1 L_2' (Λ_1) bands and the broken lines are the L_3, L_3' (Λ_3) bands. The multipoles included in each calculation are denoted by (l, n) where 'n' denotes $g(n)$ in the ascending g-values order of table 1. In (a) three multipoles are included for the L_1, L_2' (Λ_1) bands: (0, 1), (0, 2), (3, 2). For the L_3, L_3' (Λ_3) bands, four multipoles are included: (−1, 2), (−1, 3), (2, 2), (2, 3). In (b) four multipoles are included for the L_1, L_2' (Λ_1) band calculation: (0, 1), (0, 2) (0, 3), (3, 2). The L_3, L_3' (Λ_3) bands are calculated as in (a). In (c) six multipoles are included for L_1, L_2' (Λ_1) and for the L_3, L_3' (Λ_3) bands. These are indicated in the $n = 6$ column of table 5.

Γ–L line. This result reflects the particular importance of these two multipoles. However, the crossing with the L_3, L_3' bands, and in particular the large band gap at the L-point (ΔE = 0.921 eV $\gg$ 0.164 eV, the experimental value [16], indicates a deficiency. Next consider the addition of the $g(3)$ multipole. As table 5 and figure 3(b) show, the calculated band gap at the L-point is substantially reduced (E = 0.531 eV) and the Γ–L band structure has improved in that only one band crossing remains. (Note from table 5 that adding the (l, g) = (3, 3) multipole does not change the results. This is due to an accidental symmetry [6], which is manifest in figure 2(b) in that $v_3(g(3), z') = 0$.) Next consider the $g(4)$ multipole, which is added in three different ways in the $n = 4$, 5, 6 multipole entries in table 5 and figure 3(c). The resulting six-multipole calculation reproduces the correct lowest-seven-bands structure along the entire Γ–L line, the correct degeneracies at the Γ point, and the calculated band gap reduces to ΔE = 0.293 eV. This band-gap value is reasonable when compared to that in [7], figure 3. A smaller effective mass will reduce this value further. This result, coupled with the above arguments about the small contribution of all higher g-multipoles, is evidence of convergence of the calculation. Uncertainties inherent to the empirical pseudopotential parameters are believed to be of the order of $O(0.1$ eV).

6. Discussion and summary

The present method bears a similarity to the symmetrized plane-wave method (SPWM)

Table 5. Convergence of the calculated six lowest bands for 'PbSe' at the L point. In the upper part of the table are listed the number 'n' of multipoles in each calculation, and the corresponding (l, g)-labels are marked by an asterisk. The g-values are denoted by their indices as they appear in table 1, e.g., $g(1)$ is denoted by '1' in the g-column. In the lower part of the table, under each 'n' are listed the band energies and the band gap ΔE_G; the latter is defined in the notes. The corresponding band symmetries are listed in the left of entries.

		$n \Rightarrow$								$n \Rightarrow$			
l	g	3	4		5		6	l	g	2	4		6
0	1	*	*	*	*	*	*	−2	2	*	*		*
0	2	*	*	*	*	*	*	1	2	*	*		*
0	3		*		*	*	*	−2	3		*		*
0	4						*	1	3		*		*
3	2	*	*	*	*	*	*	−2	4				*
3	3				*			1	4				*
3	4			*		*	*						
D_{3d} representation		Band energies[a]						D_{3d} representation		Band energies[a]			
L_2'		10.058	9.432	9.897	9.432	9.168	8.896	L_3'		11.246	10.712	10.468	
L_1		9.137	8.901	9.013	8.901	8.749	8.603	L_3		8.593	7.180	6.414	
L_1		1.496	1.368	1.484	1.368	1.355	1.347						
L_2'		− 6.000	−6.919	−6.110	−6.919	−7.126	−7.355						
E[b]		0.921	0.531	0.884	0.531	0.419	0.293	E[c]		2.653	3.532	4.054	

[a] Energies are given in eV.

[b] $E = E(L_2' - E(L_1)$, where the two highest energies in each column are employed.

[c] $E = E(L_3') - E(L_3)$.

for band-structure calculations [17] in that the k-point symmetry is utilized to construct 'multipoles' in terms of which the secular-equation dimensionality is reduced. The present method, however, has the following new features: (1) as a consequence of introducing cylindrical coordinates, the cylindrical multipoles depend only on one coordinate, while the SPWM multipoles depend on all three coordinates; (2) the cylindrical multipoles satisfy an exact coupled set of 1D wave equations, which do not depend on the chosen basis for the calculations, e.g., the plane waves of the SPWM. On the other hand, both the SPWM and the present method are applicable only for phenomenological calculations since they do not yield the bands throughout the Brillouin zone.

This work suggests extensions in several directions. To calculate the bands of momenta near a high-symmetry axis, a generic $k \cdot p$ approximation can be straightforwardly formulated. Unlike the standard 3D $k \cdot p$ method where the three momenta components are treated perturbatively, in the present 'cylindrical' $k \cdot p$ approximation only the two transverse momenta deviations are treated perturbatively. Details are deferred to a later publication. Such an approximation scheme may be particularly suitable for interface problems, such as in ferromagnetic layers [1] and inverted semiconductor junctions. Other useful extensions are the inclusion of the spin–orbit interaction, which is deferred to another publication, and applications of the present paradigm to different high-symmetry axes and point groups that pertain to a large class of epitaxial superlattices currently fabricated. It would also be of interest to apply the method to semiconductors such as Si, for which reliable local pseudopotentials exist, and which are unencumbered by the spin–orbit interaction. Such an exercise may be relevant to the study of Si–silicide interfaces [18].

In summary, we have introduced a method for phenomenological pseudopotential band-structure calculations along a symmetry axis. The two central results of this work are the derivation of a *single-variable* wave-equation set for the cylindrical multipoles, and the demonstration of a good convergence of the multipole expansion for a test case. The former dimensionality reduction employs geometrical coefficients, the A-coefficients, which express the transverse reciprocal lattice momentum vector-addition constraints, in analogy with the Clebsch–Gordan coefficients for 3D angular-momentum addition. The convergence demonstration is essential to establish the usefulness of the present method. As is shown in sections 1 and 5, symmetry and energy considerations, supplemented by examination of the pseudopotential multipoles, are sufficient to determine the 'small' number of relevant multipoles in advance of any secular-matrix calculations. As argued in section 1, this number of relevant multipoles does *not* depend on the z'-extension of the unit cell. This statement implies that whereas the number of basis functions for a bulk calculation grows with the unit cell as N^3, where N is the number of basis functions (e.g., plane waves) needed for each direction in space, the number of basis functions in the present calculation grows with the unit cell as mN, where m represents the product of the number of relevant g- and l-values, and hence is 'small' (in the example $m = 6$). Hence for the highly anisotropic structures in one direction, e.g., superlattices the present approach is expected to be particularly advantageous.

Acknowledgments

One of us (DA) would like to acknowledge Dr E Callen for his constructive criticism and interest at the early stages of this work, and Dr G Wright for useful scrutiny and encouragement. Thanks are extended also to Drs J Cullen and T K Chu for stimulating discussions. This work was sponsored by the NSWC Independent Research Fund and the Office of Naval Research.

Appendix A

An important step in deriving the wave equation (4.2) is to express $X_l(g_0, z')$ in terms of wavefunction and pseudopotential multipoles. The starting point is the explicit expression of $X_l(g_0, z')$

$$X_l(g_0, z') = \mathrm{i}^l \sum_{G', L': |G'_T + L'_T| = g_0} v'(G')\Psi'(L')\mathrm{e}^{\mathrm{i}(L'_z + G'_z + k')z'} \mathrm{e}^{-\mathrm{i}l\delta(G'_T + L'_T)} \tag{A1}$$

where $\Psi(L') \equiv \Psi_{nk}(L')$ and the shift phase δ is defined as in (2.5). The constraint on the summation in (A1) reflects the geometry of a triangle formed by vector addition of G'_T and L'_T, (see figure 1). Specifically, for the triangle in figure 1 the cosine theorem gives

$$\cos\left[\delta(G'_T) - \delta(L'_T)\right] = (g_0^2 - g_P^2 - g_F^2)/2g_P g_F = c(g_0, g_P, g_F) \equiv c. \tag{A2}$$

The constraint summation in (A1) can now be rewritten in a more convenient form as

$$\sum_{g_P, g_F: |c(g_0, g_P, g_F)| < 1} \quad \sum_{G': |G'_T| = g_P} \quad \sum_{L': |L'_T| = g_F} \tag{A3}$$

where the notation implies a summation of g_P, g_F such that for a given g_0, $|c| < 1$ holds. Only the non-degenerate triangle case is discussed here. Further details are given elsewhere [6]. To manipulate (A1) we note first an identity. Projection of the triangle in figure 1 onto the x' and y' axes, and adding the two equalities with the imaginary unit factor, gives

$$\mathrm{e}^{\pm\mathrm{i}\delta(G'_T + L'_T)} = (1/g_0)\left[\mathrm{e}^{\pm\mathrm{i}\delta(G'_T)} + \mathrm{e}^{\pm\mathrm{i}\delta(L'_T)}\right]. \tag{A4}$$

On the other hand, inversion of (A2) gives

$$\delta(G'_T) - \delta(L'_T) = \pm\alpha \qquad \alpha = |\cos^{-1} c| \tag{A5}$$

where the two signs in (A5) correspond to the possible triangles (interchanging G'_T and L'_T) with the same $G'_T + L'_T$. Combining (A4) and (A5) yields

$$\mathrm{e}^{-\mathrm{i}l[\delta(G'_T + L'_T) - \delta(L'_T)]} = B_l^{(+)}\delta_{\delta(G'_T) - \delta(L'_T) - \alpha} + B_l^{(-)}\delta_{\delta(G'_T) - \delta(L'_T) + \alpha} \tag{A6}$$

and

$$B_1^{(+)} = (1/g_0)\left[g_F - g_P\left(c - \mathrm{i}\sqrt{1 - c^2}\right)\right] \qquad B_1^{(-)} = \left(B_1^{(+)}\right)^*. \tag{A7}$$

The Kronecker δ in (A6) follow from (A5) and the discreteness of the shift angles $\delta(G'_T)$, $\delta(L'_T)$. Furthermore, since $\alpha \neq 0$ for a non-degenerate triangle, raising both sides of (A6) to the lth power yields

$$\mathrm{e}^{-\mathrm{i}l[\delta(G'_T + L'_T) - \delta(L'_T)]} = B_l^{(+)}\delta_{\delta(G'_T) - \delta(L'_T) - \alpha} + B_l^{(-)}\delta_{\delta(G'_T) - \delta(L'_T) + \alpha} \qquad B_l^{(\pm)} = \left(B_1^{(\pm)}\right)^l. \tag{A8}$$

To express the Kronecker δ-factors in (A8) in a separable form consider their arguments. Since the shift angles $\delta(G'_T)$, $\delta(L'_T)$ satisfy (3.1), it follows that

$$\delta(G'_T) - \delta(L'_T) \pm \alpha = (\pi/3)(j - n) + \Phi_0(g_P) - \Phi_0(g_F) \pm \alpha = (\pi/3)(j - n) + \Delta^{\pm} \tag{A9}$$

where j, $n = 0, \pm 1, \pm 2, \ldots$. Now (A8) is under the G'_T, L'_T summations of (A3). Hence, at least one triangle G'_T, L'_T and $G'_T + L'_T$ is formed with $|G'_T + L'_T| = g_0$. Therefore, as a function of j and n, the RHS of (A9) vanishes for at least one configuration of the transverse reciprocal lattice vectors. Hence $\Delta^{\pm}$ must be a multiple of $\pi/3$ and the LHS of (A9) is *always* a multiple of $\pi/3$ less than 2π. Consequently, the Kronecker δ can be expressed using the identity [19]

$$\delta_{(\pi/3)s} = \frac{1}{6}\sum_{m=-2}^{3} e^{-i(\pi/3)ms} \qquad \text{for } |s| \leqslant 6. \tag{A10}$$

Replacing $(\pi/3)s$ in (A10) by the LHS of (A9), the Kronecker δ-factors attain a separable form, which then leads, after inserting in (A1), to wave equation (4.2).

References

[1] Baltenberger W and Helman I S 1990 *Appl. Phys. Lett.* **57** 2954
Hathaway K B and Cullen J R 1992 *J. Magn. Magn. Mater.* **104–107** 1840

[2] Bastard G 1981 *Phys. Rev.* B **24** 5693; 1982 *Phys. Rev.* **25** 7584; 1988 *Wave Mechanics Applied to Semiconductor Heterostructures* (New York: Halsted)

[3] See, e.g. Fong C Y 1979 *Electrons and Phonons in Layered Crystal Structures* ed T J Weiting and M Schluter (Dordrecht: Reidel) p 29
Van De Walle C G and Martin R M 1986 *Mater. Res. Soc. Symp. Proc.* vol 63 (Pittsburg, PA: Materials Research Society) p 21
Schulman J N and McGill T C 1985 *Synthetic Modulated Structures* ed L L Chang and B C Geissen (New York: Academic) p 77
Schulman J N and Chang Y C 1985 *Phys. Rev.* **31** 2056
Chang Y C and Schulman J C 1985 *Phys. Rev.* B **31** 2069

[4] Cohen M L and Heine V 1970 *Solid State Physics* vol 24 ed D Turnbull and F Seitz (New York: Academic) p 37
Cohen M L 1979 *Phys. Today* July 40

[5] Olver F W J 1964 *Handbook of Mathematical Functions (Applied Mathematics 55)* ed M Abramowitz and I A Stegun (White Oak, NY: National Bureau of Standards) p 355

[6] Agassi D and Restorff J B 1991 *Naval Surface Warfare Center Technical Report* TR91-324 (available from the National Technical Information Service, Springfield, VA 22161)

[7] See, e.g., Martinez G, Schluter M and Cohen M L 1975 *Phys. Rev.* B **11** 651

[8] Morgan D J 1969 *Solid State Theory* ed P T Landsberg (London: Wiley–Interscience) p 195

[9] Gradshteyn I S and Ryzhik I M 1965 *Table of Integrals Series and Products* (New York: Academic) p 973

[10] Ashcroft N W and Mermin N D 1976 *Solid State Physics* (New York: Holt, Rinehart and Winston) p 133

[11] Dalven R 1973 *Solid State Physics* vol 28 ed H Ehrenreich, F Seitz and D Turnbull (New York: Academic) p 183
Philips J C 1973 *Bonds and Bands in Semiconductors* (New York: Academic) p 123
Rabe K M and Joannopoulos J D 1985 *Phys. Rev.* B **32** 2302

[12] Slater J C 1965 *Quantum Theory of Molecules and Solids* vol 1 (New York: McGraw-Hill) p 315

[13] Ashcroft N W and Mermin N D 1976 *Solid State Physics* (New York: Holt, Rinehart and Winston) pp 88, 106

[14] McKelvey J P 1969 *Solid State and Semiconductor Physics* (New York: Harper and Row) p 212

[15] Kohn S E, Yu P Y, Petroff Y, Shen Y R, Tsang Y and Cohen M L 1973 *Phys. Rev.* B **8** 1477

[16] Nimtz G and Schlicht B 1985 *Narrow Gap Semiconductors* (Berlin: Springer) section 3.1

[17] Schlosser H 1962 *J. Phys. Chem.* **23** 963
Callaway J 1974 *Quantum Theory of the Solid State* vol A (New York: Academic) p 264

[18] Tromp R M, Reuter M C, LeGoues F K and Krakow W 1989 *J. Vac. Sci. Technol.* A **7** 1910

[19] Landsberg P T 1969 *Solid State Theory* ed P T Landsberg (London: Wiley–Interscience) ch B, p 71